Climate Change Initiative+ (CCI+) Phase 2

Sea Surface Salinity

Algorithm Development Plan (ADP)

Customer: ESA

Ref.: ESA-CCI-PRGM-EOPS-SW-17-0032

Version: v4.0

Revision Date: 07/11/2022

Filename: SSS_cci-D2.4-ADP_v4.0.docx

Deliverable code: D2.4

Signatures

Author	Nicolas Reul (Science Leader)		07/11/2022
Reviewed by	Rafael Catany		
Approved by	Jacqueline Boutin (Science Leader)		07/11/2022
	Nicolas Reul (Science Leader)		07/11/2022
	Rafael Catany (Project Manager)		07/11/2022
	Roberto Sabia (Technical Officer)		
Accepted by	Susanne Mecklenburg (Technical Officer) ESA		

Diffusion List
Sea Surface Salinity Team Members
ESA (Susanne Mecklenburg, Roberto Sabia)

Amendment Record Sheet

Date / Issue	Description	Section / Page
07/11/2022 / v4.0	Circulation ADP first CRDP for CCI Salinity phase 2 (April 2022 to April 2025)	New document

Table of Contents

List of figures

List of tables

No table of figures entries found.

1 Introduction

1.1 Scope of this document

This document holds the Algorithm Development Plan (ADP) prepared by CCI+ team, as part of the activities included in the [WP210] of the Proposal (Task 2 from SoW ref. ESA-CCI-PRGM-EOPS-SW-17-0032).

This document summarizes the planned algorithm developments to be performed for the CCI+SSS project phase-2 activity.

1.2 Structure of the document

This document is composed of 3 sections and present the plan for the development of the CCI-SSS algorithm that are proposed for the 1st CRDP, along to the evolution plan for the second CRDP. **Section 1** is an introduction presenting the scope, reference and applicable documents, acronyms, and the structure of the document. **Section 2** presents the plan for the algorithms of L-band sensor-based SSS algorithms and which form the core of the CCI-SSS products. In **Section 3**, we detail the algorithm development for CCI-SSS algorithms based on C and X-band data and in **Section 4**, we provide summary and next steps.

1.3 References

1.3.1 Applicable Documents

ID	Document	Reference
AD01	CCI+ Statement of Work	SoW
AD02	Product User Guide (PUG)	PUG
AD03	User Requirement Document (URD)	SSS_cci-D1.1-URD-i1r0
AD04	Product Specification Document (PSD)	SSS_cci-D1.2-PSD-v1r4
AD05	Algorithm Theoretical Baseline Document	SSS_cci-D2.3-ATBD_L3_L4-i1r0_v1.1
AD06	Algorithm Development Plan (ADP) for CCI-SSS 1st phase	SSS_cci-D2.4-ADP_v3.1

1.3.2 Reference Documents

ID	Document	Reference
RD01	Boutin, J., N. Martin, N. Kolodziejczyk, and G. Reverdin (2016a), Interannual anomalies of SMOS sea surface salinity, *Remote Sensing of Environment*	doi:http://dx.doi.org/10.1016/j.rse.2016.02.053

ID	Document	Reference
RD02	Kolodziejczyk, N., J. Boutin, J.-L. Vergely, S. Marchand, N. Martin, and G. Reverdin (2016), Mitigation of systematic errors in SMOS sea surface salinity, *Remote Sensing of Environment*	doi:http://dx.doi.org/10.1016/j.rse.2016.02.061.
RD03	Liang Hong, Normal Kuring, Joel Gales and Fred Patt (2017), AQ-014-PS-0017_Aquarius_L2toL3ATBD_DatasetVersion5.0	
RD04	Fred Patt, Liang Hong (2017), AQ-014-PS-0018_AquariusLevel2specification_DatasetVersion5.0	
RD05	Meissner, T. and F. J. Wentz, 2016: Remote Sensing Systems SMAP Ocean Surface Salinities [Level 2C, Level 3 Running 8-day, Level 3 Monthly], Version 2.0 validated release. Remote Sensing Systems, Santa Rosa, CA, USA.	www.remss.com/missions/smap, doi:10.5067/SMP20-2SOCS
RD06	Boutin J., J.-L. Vergely, S. Marchand, F. D'Amico, A. Hasson, N. Kolodziejczyk, N. Reul, G. Reverdin, J. Vialard (2018), New SMOS Sea Surface Salinity with reduced systematic errors and improved variability, *Remote Sensing Of Environment*	doi:http://dx.doi.org/10.1016/j.rse.2018.05.022
RD07	Yiwen Zhou ; Roger H. Lang ; Emmanuel P. Dinnat ; David M. Le Vine (2017), L-Band Model Function of the Dielectric Constant of Seawater, *IEEE Transactions on Geoscience and Remote Sensing* (Volume: 55 , Issue: 12)	
RD08	Gaillard F. (2015), ISAS-13 temperature and salinity gridded fields. SEANOE.	http://doi.org/10.17882/45945.
RD09	Reul Nicolas, Saux Picart Stephane, Chapron Bertrand, Vandemark D., Tournadre Jean, Salisbury J. (2009). Demonstration of ocean surface salinity microwave measurements from space using AMSR-E data over the Amazon plume. Geophysical Research Letters (GRL) , 36, 1-5 .	https://doi.org/10.1029/2009GL038860
RD10	Qingtao Song and Zhaohui Wang. (2017). Sea surface salinity observed from the HY-2A satellite. Satellite Oceanography and Meteorology, vol.2 (1): 41–48.	http://dx.doi.org/10.18063/SOM.2017.01.004.
RD11	Wentz, F. J., and T. Meissner (2000), AMSR ocean algorithm, version 2, algorithm theoretical basis document, RSS Tech. Rep. 121599A-1, Remote Sens. Syst., Santa Rosa, Calif.	
RD12	Wentz, F. J. and T. Meissner, (2007), AMSR-E Ocean Algorithms; Supplement 1, report number 051707, 6 pp., Remote Sensing Systems, Santa Rosa, CA.	
RD13	Meissner, T., and F. J. Wentz, (2012), The emissivity of the ocean surface between 6 - 90 GHz over a large range of wind speeds and Earth incidence angles, IEEE TGRS, 50(8), 3004-3026.	
RD14	Webster, W. J., T. T. Wilheit, D. B. Ross, and P. Gloersen (1976), Spectral characteristics of the microwave emission from a wind-driven foam-covered sea, J. Geophys. Res., 18, 3095–3099.	
RD15	Dinnat, E.P.; Le Vine, D.M.; Boutin, J.; Meissner, T.; Lagerloef, G. Remote Sensing of Sea Surface Salinity: Comparison of Satellite and In Situ Observations and Impact of Retrieval Parameters. *Remote Sens.* **2019**, *11*, 750.	

ID	Document	Reference
RD16	Olivier, L., G. Reverdin, A. Hasson, and J. Boutin (2020), Tropical Instability Waves in the Atlantic Ocean: Investigating the Relative Role of Sea Surface Salinity and Temperature From 2010 to 2018, Journal of Geophysical Research: Oceans, 125(12), e2020JC016641, doi:https://doi.org/10.1029/2020JC016641	
RD17	Akhil, V. P., J. Vialard, M. Lengaigne, M. G. Keerthi, J. Boutin, J. L. Vergely, and F. Papa (2020), Bay of Bengal Sea surface salinity variability using a decade of improved SMOS re-processing, Remote Sensing of Environment, 248, 111964, doi:https://doi.org/10.1016/j.rse.2020.111964.	
RD18	Reverdin, G., et al. (2021), Formation and Evolution of a Freshwater Plume in the Northwestern Tropical Atlantic in February 2020, Journal of Geophysical Research: Oceans, 126(4), e2020JC016981, doi:10.1029/2020jc016981.	
RD19	Kerr, Y., et al. (2019), Low Frequency Passive Microwave User Requirement Consolidation Study, Issue 2,*Rep. SO-TN-CB-GS-0075*, CESBIO, Toulouse, https://mycore.core-cloud.net/index.php/s/Y3tpySnNhI9HWUH	
RD20	Fournier, S., and T. Lee (2021), Seasonal and Interannual Variability of Sea Surface Salinity Near Major River Mouths of the World Ocean Inferred from Gridded Satellite and In-Situ Salinity Products, Remote Sensing, 13(4), 728.	
RD21	Yu, L., F. M. Bingham, T. Lee, E. P. Dinnat, S. Fournier, O. Melnichenko, W. Tang, and S. H. Yueh (2021), Revisiting the Global Patterns of Seasonal Cycle in Sea Surface Salinity, Journal of Geophysical Research: Oceans, 126(4), e2020JC016789, doi:https://doi.org/10.1029/2020JC016789.	
RD22	Bingham, F. M., S. Brodnitz, and L. Yu (2021), Sea Surface Salinity Seasonal Variability in the Tropics from Satellites, Gridded In Situ Products and Mooring Observations, Remote Sensing, 13(1), 110.	
RD23	Melnichenko, O., P. Hacker, N. Maximenko, G. Lagerloef, and J. Potemra (2016), Optimum interpolation analysis of Aquarius sea surface salinity, Journal of Geophysical Research: Oceans, 121(1), 602-616, doi:https://doi.org/10.1002/2015JC011343.	
RD24	Nardelli, B., R. Droghei, and R. Santoleri (2016), Multi-dimensional interpolation of SMOS sea surface salinity with surface temperature and in situ salinity data, Remote Sensing of Environment, 180, 392-402, doi:https://doi.org/10.1016/j.rse.2015.12.052.	
RD25	Kolodziejczyk, N., M. Hamon, J. Boutin, J.-L. Vergely, G. Reverdin, A. Supply, and N. Reul (2021), Objective Analysis of SMOS and SMAP Sea Surface Salinity to Reduce Large-Scale and Time-Dependent Biases from Low to High Latitudes, Journal of Atmospheric and Oceanic Technology, 38(3), 405-421, doi:10.1175/jtech-d-20-0093.1.	
RD26	Boutin, J., J.-L. Vergely, E. P. Dinnat, P. Waldteufel, F. D'Amico, N. Reul, A. Supply, and C. Thouvenin-Masson (2021), Correcting Sea Surface Temperature Spurious Effects in Salinity Retrieved From Spaceborne L-Band Radiometer Measurements, IEEE Transactions on Geoscience and Remote Sensing, 59(9), 7256-7269, doi:10.1109/tgrs.2020.3030488.	
RD27	Kao, H.-Y., G. S. E. Lagerloef, T. Lee, O. Melnichenko, T. Meissner, and P. Hacker (2018), Assessment of Aquarius Sea Surface Salinity, Remote Sens., 10(9):1341.	
RD28	Fournier, S., T. Lee, X. Wang, T. W. K. Armitage, O. Wang, I. Fukumori, and R. Kwok (2020), Sea Surface Salinity as a Proxy for Arctic Ocean Freshwater Changes, Journal of Geophysical Research: Oceans, 125(7), e2020JC016110, doi:https://doi.org/10.1029/2020JC016110.	

ID	Document	Reference
RD29	Brucker, L., E. P. Dinnat, and L. S. Koenig (2014), Weekly gridded Aquarius L-band radiometer/scatterometer observations and salinity retrievals over the polar regions – Part 2: Initial product analysis, The Cryosphere, 8(3), 915-930, doi:10.5194/tc-8-915-2014.	
RD30	Olmedo, E., C. Gabarró, V. González-Gambau, J. Martínez, J. Ballabrera-Poy, A. Turiel, M. Portabella, S. Fournier, and T. Lee (2018), Seven Years of SMOS Sea Surface Salinity at High Latitudes: Variability in Arctic and Sub-Arctic Regions, Remote Sensing, 10(11), 1772	
RD31	Supply, A., J. Boutin, J.-L. Vergely, N. Kolodziejczyk, G. Reverdin, N. Reul, and A. Tarasenko (2020b), New insights into SMOS sea surface salinity retrievals in the Arctic Ocean, Remote Sensing of Environment, 249, 112027, doi:https://doi.org/10.1016/j.rse.2020.112027.	
RD32	Tang, W., S. Yueh, D. Yang, A. Fore, A. Hayashi, T. Lee, S. Fournier, and B. Holt (2018), The Potential and Challenges of Using Soil Moisture Active Passive (SMAP) Sea Surface Salinity to Monitor Arctic Ocean Freshwater Changes, Remote Sensing, 10(6), 869.	
RD33	Vazquez-Cuervo, J., C. Gentemann, W. Tang, D. Carroll, H. Zhang, D. Menemenlis, J. Gomez-Valdes, M. Bouali, and M. Steele (2021), Using Saildrones to Validate Arctic Sea-Surface Salinity from the SMAP Satellite and from Ocean Models, Remote Sensing, 13(5), 831.	
RD34	Tarasenko, A., A. Supply, N. Kusse-Tiuz, V. Ivanov, M. Makhotin, J. Tournadre, B. Chapron, J. Boutin, N. Kolodziejczyk, and G. Reverdin (2021), Properties of surface water masses in the Laptev and the East Siberian seas in summer 2018 from in situ and satellite data, Ocean Sci., 17(1), 221-247, doi:10.5194/os-17-221-2021.	
RD35	Supply, A., J. Boutin, J.-L. Vergely, N. Martin, A. Hasson, G. Reverdin, C. Mallet, and N. Viltard (2018), Precipitation Estimates from SMOS Sea-Surface Salinity, Quarterly Journal of the Royal Meteorological Society, 144(S1), 103-119, doi:https://doi.org/10.1002/qj.3110.	
RD36	Supply, A., J. Boutin, G. Reverdin, J.-L. Vergely, and H. Bellenger (2020a), Variability of Satellite Sea Surface Salinity Under Rainfall, in Satellite Precipitation Measurement: Volume 2, edited by V. Levizzani, C. Kidd, D. B. Kirschbaum, C. D. Kummerow, K. Nakamura and F. J. Turk, pp. 1155-1176, Springer International Publishing, Cham, doi:10.1007/978-3-030-35798-6_34.	
RD37	Hasson, A., M. Puy, J. Boutin, E. Guilyardi, and R. Morrow (2018), Northward Pathway Across the Tropical North Pacific Ocean Revealed by Surface Salinity: How do El Niño Anomalies Reach Hawaii?, Journal of Geophysical Research: Oceans, 123(4), 2697-2715, doi:https://doi.org/10.1002/2017JC013423.	
RD38	Boutin, J., N. Martin, G. Reverdin, S. Morisset, X. Yin, L. Centurioni, and N. Reul (2014), Sea surface salinity under rain cells: SMOS satellite and in situ drifters observations, Journal of Geophysical Research: Oceans, 119(8), 5533-5545, doi:https://doi.org/10.1002/2014JC010070	

1.4 Acronyms

AD	Applicable Document
ATBD	Algorithm Theoretical Basis Document
Aquarius	NASA mission

CCI	The ESA Climate Change Initiative (CCI) is formally known as the Global Monitoring for Essential Climate Variables (GMECV) element of the European Earth Watch programme
CCI+	Climate Change Initiative Extension (CCI+), is an extension of the CCI over the period 2017–2024
CMEMS	Copernicus Marine Environmental Monitoring Service
CRDP	Climate Research Data Package
DARD	Data Access Requirements Document
DOI	Digital Object Identifier
DPM	Detailed Processing Model
ECMWF	European Centre for Medium Range Weather Forecasts
ECV	Essential Climate Variable
EO	Earth Observation
FOV	Field Of View
Hs	Significant Wave Height (see also SWH)
KS	Klein and Swift sea water dielectric constant model
MW	Meissner and Wentz sea water dielectric constant model
NASA	National Aeronautics and Space Administration
NOAA	National Oceanic and Atmospheric Administration
NOP	Numerical Ocean Prediction
NWP	Numerical Weather Prediction
OTT	Ocean Target Transform
SSS	Sea Surface Salinity
SST	Sea Surface Temperature
SWH	Significant Wave Height (see also Hs)
TBC	To Be Completed
UCR/CECR	Uncertainty Characterisation Report (formerly known as the Comprehensive Error Characterisation Report)
URD	User Requirements Document
VOS	Volunteer Observing ships
WS	Wind Speed

2 Plan for L-band data based CCI+SSS Algorithms

2.1 Input Level 2/Level 3 Data

For the 1st CRDP of CCI+SSS phase 2, the input data to the CCI algorithms are levels 2 for SMOS and SMAP or Level 3 for Aquarius sensor. These data are all projected on the CCI+SSS Level 4 grids (see Section below). The input data are the following for each sensor:

- **SMOS:** for the global products, we will use as input L2 products generated by the SMOS ESA L2 v700 chain. These products are provided onto an ISEA grid at 15km resolution. SSS is classified according to the distance to the sub-satellite track and into ascending and descending passes. For polar products, we will also test the use of polar CCI level 2 SSS produced during phase 1 (v671 obtained from ERA5 auxiliary data over polar grids). Several retrieved SSS will be tested (SSS retrieved with or without wind speed retrieval, as tested in v671 retrievals).
- **SMAP:** as in CCI+SSS phase 1, we will use the RSS Level 2 v5.0 products. These are swath SSS from SMAP provided daily at 40 km resolution. The data are split into ascending and descending products and between the fore and aft views.
- **Aquarius:** as in CCI+SSS phase 1, we will use as input the official release products L3 v5.0, which is the official end of mission public data release from the AQUARIUS/SAC-D mission. Daily Aquarius Level 3 sea surface salinity (SSS) at 1-degree spatial resolution are used.

2.2 Grid change

During CCI+SSS phase 1, L3 and L4 products were generated on the EASE equatorial grid. Following users' recommendations and feedback, during CCI+SSS phase 2, L3 products will be delivered on a 0.25° regular grid. L4 products will be delivered on a 0.25° regular grid and on two polar EASE grids, one for high northern latitudes, one for high southern latitudes.

The projection algorithms on the 3 above mentioned grids depend on the input product:

- SMOS and SMAP data are reprojected using a nearest neighbour criteria.

- For Aquarius data set, the current phase 1 interpolation will be kept. It is a weighting of the 4 nearest neighbours according to the inverse of the square of the distance.

2.3 Level 2 preconditioning

Pre-processing algorithms will be developed in particular to correct some seasonal latitudinal biases and to mitigate some intermittent RFI biases.

2.3.1 Seasonal biases correction.

During phase 1, significant seasonal biases appeared at intermediate and high latitudes. These biases affect all sensors. They have been partially corrected on SMOS and not at all on Aquarius and SMAP.

On SMOS, they have been corrected by self-referencing (latitudinal seasonal correction). We propose to correct them by taking ISAS as reference. The same will be done for SMAP and Aquarius.

For the new polar products, several approaches will be investigated. At very high latitudes, ISAS is not well suited to serve as a reference (ISAS is very poorly constrained due to the lack of in situ measurements). It is a matter of self-referencing by identifying the sensor(s) that are the least affected by seasonal biases mainly related to the presence of the ice vicinity. These biases are particularly important because of the very low SST encountered in these regions. These seasonal biases cannot be properly corrected latitudinally. Therefore, a grid node by grid node seasonal correction approach is considered. Two different ways will be tested for the calculation of this correction depending on how the SMOS-SMAP-Aquarius data are collocated. Indeed, it is possible to compare the data on a monthly or weekly average basis. Weekly averages would better account for the intra-monthly variability of the ice edge position.

2.3.2 RFI mitigation.

The RFIs mainly affect SMOS and to a much less extent SMAP and Aquarius. We propose to implement an algorithm that allows correcting the temporal variations of RFI biases based on a regional principal component analysis (PCA). This correction is estimated according to the across-swath position, to the orbit orientation and the region considered. It is then applied on the SMOS levels 2 and gives rise to L2 intermediate products. These intermediate products are the input of the L3 and L4 algorithms.

For the first CRDP, this correction will be applied on two or three regions only.

This correction is not applied on Aquarius nor on SMAP.

2.4 Plan for L3 algorithms

L3 products will be derived using the same methodology as in CCI+SSS phase 1.

They are, by definition, time and space-averaged products obtained sensor by sensor, without mixing inter-sensor information. Here, we consider simple averages of swath Level 2 SSS products, which may have been already corrected for some biases (e.g. land sea contamination or spatio-temporal drifts corrections in the brightness temperatures of the instrument such as the Ocean Target Transformation). These products can thus be used as a reference in terms of observed SSS variability since we don't apply to the observed SSS any specific smoothing operation (for example, by allowing introducing representativity errors or variance filtering).

A priori, these products will not be distributed to users except upon specific requests. They will be made available as part of the validation and verification of products and will serve to build up the Level 4 products.

They will be delivered on a 0.25° regular grid (same grid as L4 products).

The space-time aggregation of the input data will be calculated for each grid node and on a daily or 10-day temporal sliding window. Using an average weighted by the errors σ_i^2 of each SSS product.

The monthly L3 products contain the averaged SSS field and the associated uncertainty for each L-band sensor: SMOS, Aquarius and SMAP.

2.5 Plan for L4 algorithms

2.5.1 Data coverage

During CCI+SSS phase 1, the data coverage was found to be insufficient, especially at high latitudes. The filtering algorithms will be modified to increase the data coverage.

2.5.2 Global L4 product algorithm

The algorithm for merging the various products will be mostly in line with the one used during phase 1.

This algorithm is a Bayesian optimal interpolation that takes into account:

-the uncertainties of the input L2 products

-the a priori variability on the SSS fields

-the representativeness errors

The Phase 1 algorithm simultaneously estimates the inter-sensor biases and the SSS time series grid node by grid node. The biases are considered constant over time.

We propose to implement a change in the algorithm in order to be able to take into account biases that vary in time. To do so, we will consider predefined periods on which the bias is constant but can differ from one period to another. The algorithm ensures the continuity of the SSS between periods. Once implemented, we will decide whether or not to use it for the generation of L4 products.

2.5.3 L4 polar algorithm

After correcting for seasonal bias (see Section 2.3.1) at Level 2, an OI identical to that of Phase 1 will be conducted. Several strategies will be tested:

-different seasonal corrections

-use of the estimated SSS with or without wind speed retrieval

- use of the estimated SSS with or without seasonal correction

- use of the estimated SSS with or without absolute bias correction

2.5.4 L4 products content and coverage

In the first CRDP, the global product will cover the period 01/2010-10/2022. The research polar product will either cover the period 01/2010-11/2020 if based on the SMOS v671 L2 product or the same period as the global product if the latter is of at least as good quality as v671 derived polar product.

As in CCI phase 1, the following fields will be included in the L4 products:

-monthly and weekly SSS fields: obtained from OI algo

-SSS uncertainty: obtained from OI algo

-number of outliers over the considered time interval (+/-30 days for monthly data and +/-10 days for weekly data).

-number of data over the considered time interval (+/-30 days for monthly data and +/-10 days for weekly data).

-SSS quality flag

-ice flag

-pct_var : 100x(SSS error)^2/variability (%)

These values will be given for each grid node and sampled every two weeks for monthly products and every day for weekly products.

2.6 Plan for the evolution of the L-band CCI algorithms for 2nd CRDP

For the CRDP 2, we plan to adjust some components of the radiative transfer model used in the SMOS SSS retrieval and to rerun the L2OS processor using SMOS L1 v7, ERA5 auxiliary parameters and ISAS to derive SMOS OTT, in order to get a more stable SMOS SSS time series. Adjustments of L2OS processor will be based on:

- new L2OS model components studied in the frame of the ESLs (roughness model and dielectric constant models),

-possible evolution of the roughness model to consider possible systematic differences between ERA5 and ECMWF forecasts auxiliary parameters

-possible evolution of the roughness model to adjust SMOS, SMAP and Aquarius models based on colocations of Tb (we do not foresee to reprocess SMAP and AQUARIUS SSS but a SSS correction based on the so-called DSSStheo approach (as described in the CCI phase 2 proposal) might be envisaged).

Other evolutions of the L2 and L4 algorithms will be studied to answer as much as possible feedbacks from the climate users about the first CRDP of CCI+SSS phase 2.

It is worth noting that the planned work is primarily aimed at algorithmic improvements based on the satellite data already acquired. In case the SMOS or SMAP instrument would stop working, the activities would be little impacted, and the time series would continue to be produced but with a lower quality during the period with only one instrument. If both instruments ceased to operate, the time series would be discontinued, but the planned work would continue to be relevant.

3 Plan for C- and X-band data based CCI SSS algorithm

3.1 Introduction and Summary of phase-1 achievements

Before 2010, in situ measurements were the only source of SSS estimates. Argo profiler data is the main source of basins-scale SSS salinity data, and Argo data was extremely sparse in the major tropical river plume regions, such as the Amazon-Orinoco, Mississippi, Congo/Niger or the Bay of Bengal river plume regions, particularly before 2002. The accumulation of Argo and previous hydrological data over time now allows depicting the seasonal variations of SSS in these regions very well. On the other hand, the Argo network coverage was insufficient to produce basin-scale seasonal SSS maps, and hence unable to describe SSS interannual variations before the advent of SSS remote sensing. Satellite SSS observation only started with ESA's SMOS (2010-now), followed by NASA's Aquarius (2011-2015) and SMAP (2015-now) missions. These three satellites are all equipped with microwave radiometers operated at L-band (central frequency ~1.4 GHz) a frequency for which the response of the sea surface emissivity to SSS is highest. While the SMOS SSS retrievals were initially highly contaminated by radio-frequency interferences and other sources of land contamination, improved bias corrections later allowed strongly improved SMOS SSS retrievals with roughly similar performances to Aquarius and SMAP, with correlations and rms-differences to co-located in situ data of 0.8, and 0.6 pss, respectively, in average in the four above mentioned regions. Data from the SMOS, Aquarius, and SMAP radiometers then allowed to describe interannual SSS signals. Yet, the SSS satellite record (12 years) is too short to confidently describe interannual SSS signals, or SSS variability on longer time scales, such as the long-term freshening expected in these regions due to the expected hydrological cycle intensification in response to anthropogenic forcing. This is mainly because of sparse in situ observations prior the full deployment of the Argo float network and the relatively recent L-band satellite radiometer era.

The Advanced Microwave Scanning Radiometer - Earth Observing System (AMSR-E) onboard Aqua satellite has microwave channels spanning the 6.9 - 89.0 GHz range (including the 6.9 (C-band) and 10.7 GHz (X-band) frequencies). AMSR-E was initially designed for monitoring atmospheric water, SST, and surface winds over the ocean. However, the C- and X-band channels also display some sensitivity to SSS at high SST, although much weaker than at L-band In fact, at the AMSR-E incidence angle of 55° and at an SST ~30°C, the perfectly flat sea surface brightness temperature sensitivity to SSS in vertical polarization is $\partial Tb/\partial SSS$ ~-0.05 K/pss, and less than -0.01 K/pss , for C- and X- band, respectively, against ~0.9 K/pss at L-Band (Reul et al., 2009). Reul et al., (2009) noted that C- and X- bands have a roughly similar sensitivity to SST and surface roughness, and that the C- minus X-band emissivity contrast keeps sensitive to SSS (~0.05 K/pss) and is much less affected by SST and surface roughness. They used that approach to estimate SSS in the Amazon River plume region. This is made possible by the high SST (which maximize the sensitivity to SSS) and strong salinity contrasts (because the low sensitivity results in a poor accuracy). Such principle has recently been applied to retrieve SSS from HY2-A data for the freshwater runoff near the Yangtze Delta. The Congo-Niger, Mississippi, and BoB also displays high SST (with most of the basin above 20 °C all year long) and very strong salinity contrasts. In this project, we investigate if the concept of Reul et al. (2009) can be applied to AMSR-E C/X bands data to reconstruct SSS over the 2002-11 period, hence yielding an almost 20-year-long satellite SSS record. Note that HY-2A was launched in 2011. Note also that WindSat's radiometer performed C- and X-band brightness temperature measurements since 2003 [23] but which are not publicly available. Hence, the datasets from both sensors are not considered for the 1st CRDP of CCI-SSS project.

The algorithm is mainly based on the Radiative Transfer Model (RTM) of Meissner and Wentz (hereafter MW12) and was described in detail in [AD 06]. Necessary empirical adjustments to the RTM and the empirical inversion model linking the C- minus X-band emissivity to SSS were first developed in phase-1. Those were specifically determined for each of the river plume region's conditions using co-located brightness temperatures (T_B), surface wind, water vapor, cloud liquid water, and SST data from AMSR-E, as well as SSS data from SMOS and Aquarius/SAC-D, all collected during the common operation period of AMSR-E and SMOS satellites (June 2010-September 2011). These algorithms were then used to produce monthly-averaged SSS fields for each region, at a spatial resolution of ~60 km and gridded at ¼°x¼° from May 2002 to Sep 2011.

During CCI-SSS project phase-1,

- we developed first algorithms to retrieve monthly 0.25°x0.25° SSS from AMSR-E data for four specific river plumes dominated warm oceanic regions (AORP, MRP, CNRP, and BoB)

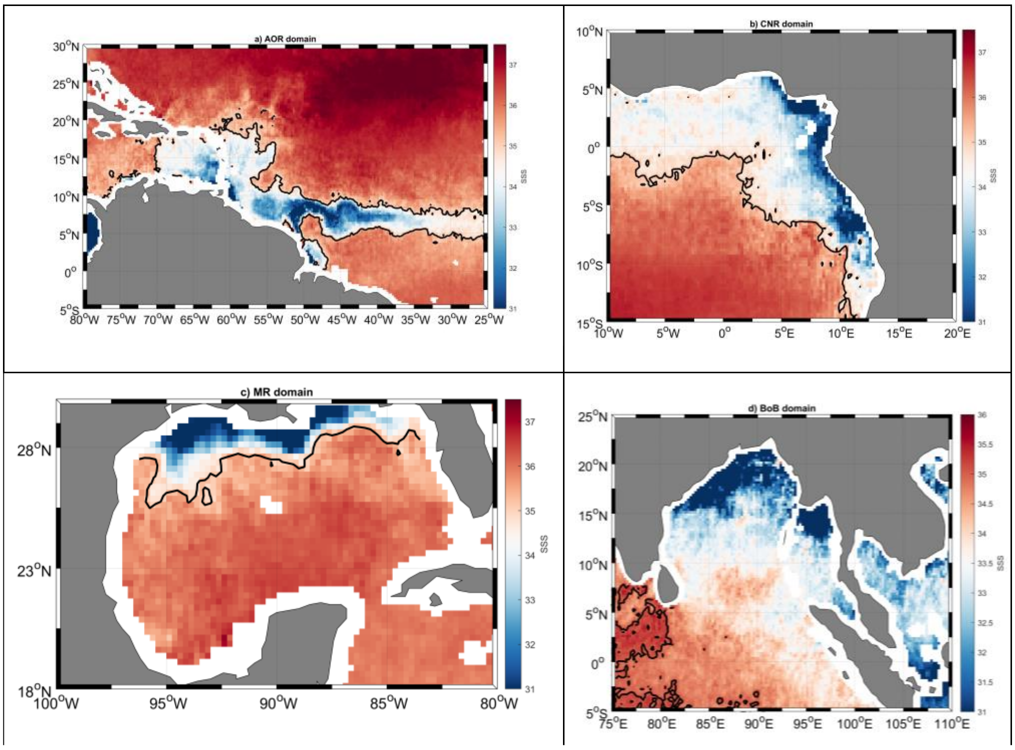

- Several algorithms options were investigated (additional empirical refinements wrt Wentz & Meissner 2012's ATBD) and several types of SSS inversion algorithm (empirical GMF, Neural Network) were tested

- Both ascending and descending passes surface emissivity frequency differential contrasts were merged as input to the algorithm,

- The auxiliary SST products used in the phase-1 algorithms is the CCI SST ESA Sea Surface Temperature Climate Change Initiative (SST_cci): Level 4 Analysis Climate Data Record, version 2.1.

- The 21 monthly maps of CCI L-band SSS v3.21 data from January 2010 to September 2011, common with AMSR-E, have been used to train the algorithms

- We finally selected a two layer feed-forward neural network (NN) with 40 Neurones per layers for each region. We used a Bayesian Regularized Artificial Neural Networks to regularize the Network towards reducing bias and variance. (A high-variance state is a state when the network is overfitted). So far, we have tested NN with 2 hidden layers and 40 Neurones per layers using as input data the surface emissivity frequency differential contrasts after atmospheric corrections and the extra polynomial empirical adjustments (wind, sst, clw, wv). Retrieval tests will be conducted in phase-2 with, or without these extra polynomial empirical adjustments to determine in which conditions do the NN inversion performs better. As found, one of the remaining issue is the relatively low number of training observations for the freshest SSS which lead, in parts, to overestimation of SSS from AMSR-E in the freshest SSS zones. To better characterize these conditions, the distance to coast has been further used as an input to the NN. Verification over the common period exhibit a 0.3-0.6 pss RSMSD between the training CCI SSS and the retrieved AMSR-E SSS.

- The data of the full AMSR-E operation period (Oct 2002-Sep 2011) have been processed at Ifremer to generate monthly first 'research' products.

- These first products were validated against in situ data from the CORA database over 2002-2009. Note that we found that the CORA datasets in these regions are still including some spurious SSS observations (in particular TSG data) that were not filtered out for a rough assessment of the AMSR-E SSS. First analyses revealed that the root Mean Square Difference (RMSD) between AMSR-E based and in situ SSS is found to be about twice the RMSD between L-band CCI v3.2 SSS and in situ in the four regions. As found, one of the major remaining issue is the systematic overestimation of the freshest SSS by the NN inversion, whatever the region.

3.2 Plan for the evolution of the C/X-band CCI algorithms for 1st CRDP

At the beginning of phase 2, we found significant differences in the spatio-temporal variability of the estimated sea surface brightness temperature frequency differential contrasts ΔTb between ascending and descending passes for all four river plume regions. These differences are particularly evident along the coastlines within a band of about ~150 kms from the nearest coastlines. This is illustrated for the Amazon and Orinoco River plume region in Figure 1 showing the differences in the temporal Median Absolute Deviation in between ascending and descending passes:

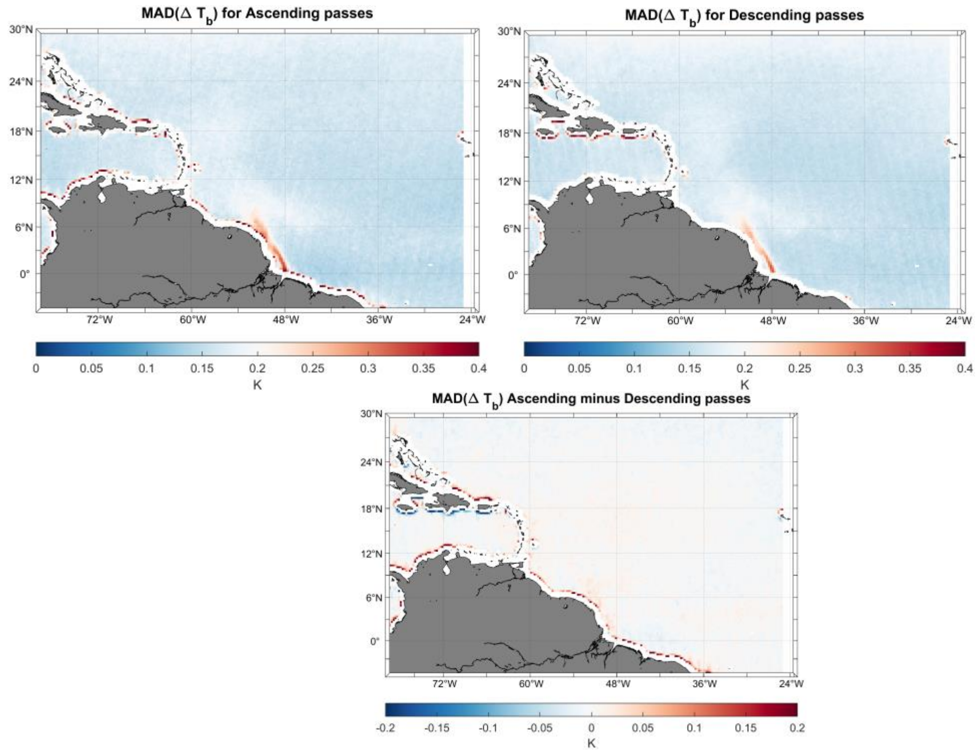

Figure 1: Temporal MAD over may 2002 to October 2011 of the surface brightness temperature frequency differential contrasts ΔTb for ascending (Top left) and descending passes (Top right). Bottom: difference between ascending and descending passes MAD.

As found, the temporal MAD over May 2002 to October 2011 of the surface brightness temperature frequency differential contrasts ΔTb is showing a similar signal associated with the Amazon River plume in both ascending and descending passes. However, a different signal variability is observed within a band following the coastlines with higher variability found north and south of the coastlines for ascending, and descending passes, respectively, as illustrated in Figure 1, bottom plot. Very similar type of behaviours were found for the 3 other remaining regions (not shown here). This evidences a potential remaining land contamination in the AMSR-E Tb data. As these potentially contaminated data were not filtered out in phase-1 for developing the NN retrievals and as high ΔTb contrasts are associated with low SSS, this issue could explain part of the systematic overestimation of the freshest SSS by the NN inversion.

The plan for the algorithm development of the first CDRP of phase-2 therefore includes a first step:

Step 1) filtering out/masking the input ΔTb where the MAD strongly differ between ascending and descending passes before training the NN.

In addition, looking back at AMSR-E SST products, we also realized that the diurnal cycles in SST might be particularly important in the studied regions (see examples for the BoB in Figure 2).

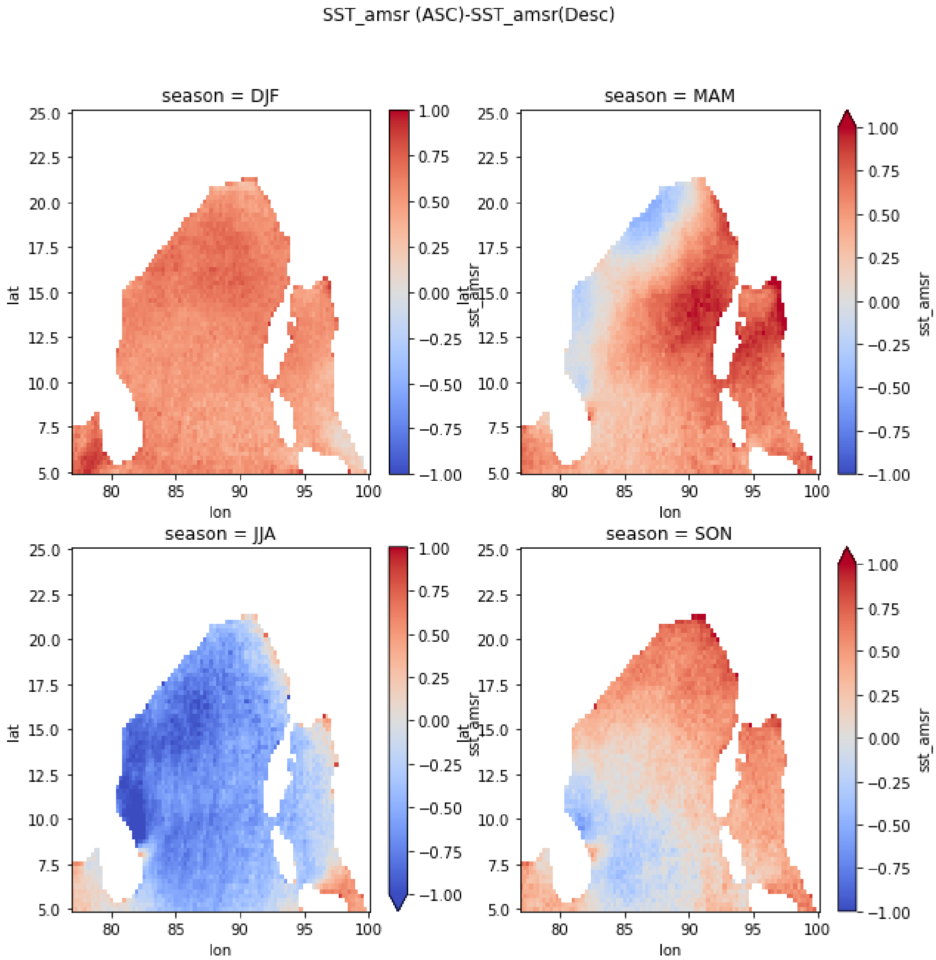

Figure 2: Mean differences between AMSR-E L2B SST retrieved in ascending (1:30 pm local time) and descending passes (1:30 am local time) for the four seasons and the BoB.

As the auxiliary SST products used as input to our NN algorithm, in phase-1, we used the CCI SST ESA Sea Surface Temperature Climate Change Initiative (SST_cci): Level 4 Analysis Climate Data Record, version 2.1. This product is based on IR data only and is adjusted to a 25 cm depth and corresponds to a nighttime 'mean' SST. Given that 1) the penetration depth at C- and X-band is ~1 cm and 2) that the ascending passes are measurements conducted at a local time of 1:30 pm, strong biases can be expected using the CCI L4 SST IR daily data as an input to our algorithm. The reason why we choose such product is a) to develop cross-ECV activities and 2) this SST analysis is independent from AMSR-E SST data themselves. Note that an SSS monthly climatology (World Ocean Atlas, [28]) is used to correct for the average SSS impact on the AMSR-E brightness temperature used in the SST retrieval. In phase-2, first CDR, given the above consideration, we now plan a second step:

Step 2) use AMSR-E SST as input to the NN SSS inversion algorithms, instead of CCI SST and assess the impact on retrieved SSS quality.

As both Land Sea contamination and diurnal cycles (SST, wind, water vapour, etc..) affect ascending and descending passes differently, it might be better for each region to develop NN inversion algorithms separately for ascending and descending passes than by combining the data from both type of passes. We plan the following development step:

Step 3) NN Retrieval tests will be conducted for ascending and descending passes separately or by merging both passes to determine in which conditions do the NN inversion performs better.

In phase-1, we developed an ensemble of empirical (polynomial) adjustments to the MW's12 RTM model including wind, SST, cloud liquid water, and water vapour corrections. We determined these functions from a residual analyses of the ΔTbs using the 21 month common period between CCI L-band SSS and AMSR-E data:

Step 4) Retrieval tests will be conducted with, and without, these extra polynomial empirical adjustments to determine in which conditions do the NN inversion performs better than our empirical fitting functions based on residual data analyses.

Finally, in phase-1, we validated the output of the first NN inversion algorithms using CORA datasets which are including some spurious SSS observations (in particular TSG data). To characterize the error in our first CRDP C/X-band SSS products we shall:

Step 5) use the EN4 validated data to best estimate the NN L3 SSS errors and to define quality levels (e.g. as a function of distance to coast, wind regimes, etc ...)

As found, one of the remaining issue is the systematic overestimation of the freshest SSS. This bias was found systematically in all four regions and using either an empirical bivariate inversion algorithm SSS=f(ΔTb, SST), or the NN inversion methods. It is likely that part of these biases are associated with the spatial sampling of AMSR-E with respect to in situ local sampling. A detail analysis of the spatio-temporal representatitivity errors of AMSR-E SSS is therefore needed. We will therefore conduct:

Step 6) Analyses of the representativity error will be conducted for the specific spatial (~60 km) and temporal resolution (monthly) of AMSR-E SSS using high resolution (1/36°) model outputs in the four regions.

3.3 Algorithm plan for C-/X-band L3 SSS of the 2nd CRDP of phase-2

For the 2nd CRDP of phase-2, we plan three major steps:

Step 1: Refine algorithms (NN) developed for the four above regions if/when needed (fresh SSS bias)

Step 2: extension to other potential regional River plume regions including Yangtze and Mekong river plumes.

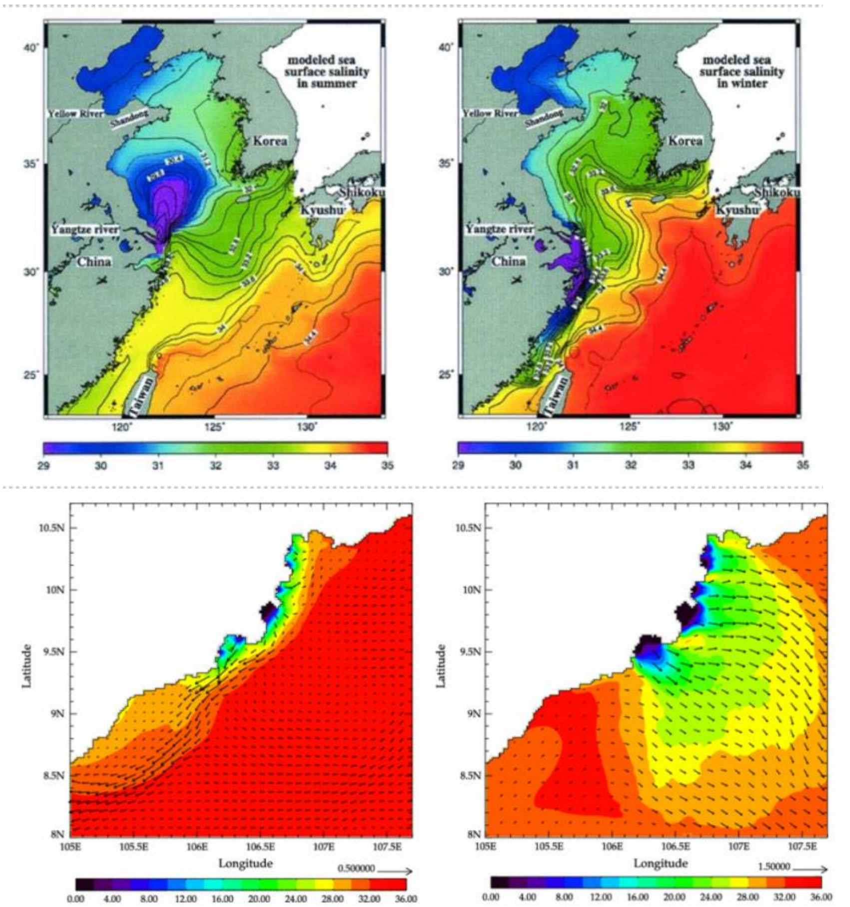

Figure 3: Top :Yangtze river plume region. Bottom: Mekong River Plume

These are very challenging regions because of potential coastal contaminations, RFI contaminations (both in C- and L-band) and because the Yangtze river plume region can exhibit cold waters in winter (< 10°C). However, these regions show very large seasonal SSS gradients and could be potentially well monitored with AMSR-E.

Step 3: consolidate the regional AMSR-E products by adding/merging WindSat-based SSS retrievals if the WindSAT Tb can be made available through ESA.

4 Summary and way forward

4.1 CCI L-band global and polar phase 2 SSS plan

During CCI+SSS phase 1, L3 and L4 products were generated on the EASE equatorial grid. During CCI+SSS phase 2, L3 products will be delivered on a 0.25° regular grid.

Pre-processing algorithms will be developed for L2 data in particular to correct some seasonal latitudinal biases and to mitigate some intermittent RFI biases. During phase 1, significant seasonal biases appeared at intermediate and high latitudes. These biases affect all sensors. They have been partially corrected on SMOS and not at all on Aquarius and SMAP. A similar self-referencing method than the one used for SMOS using ISAS fields will be applied in phase-2 for SMAP and Aquarius. For the new polar products, several approaches will be investigated. The RFIs mainly affect SMOS and to a much less extent SMAP and Aquarius. We propose to implement an algorithm that allows correcting the temporal variations of RFI biases based on a regional principal component analysis (PCA). For the first CRDP, this correction will be applied on two or three regions only and for SMOS only.

L3 products will be derived using the same methodology as in CCI+SSS phase 1. A priori, these products will not be distributed to users except upon specific requests. They will be made available internally as part of the validation and verification of products and will serve to build up the Level 4 products.

During CCI+SSS phase 1, the L4 data coverage was found to be insufficient, especially at high latitudes. The filtering algorithms will be modified to increase the data coverage. The algorithm for merging the various products will be mostly in line with the one used during phase 1. We propose however to implement a change in the algorithm in order to be able to take into account biases that vary in time. To do so, we will consider predefined periods on which the bias is constant but can differ from one period to another. The algorithm ensures the continuity of the SSS between periods. Once implemented, we will decide whether or not to use it for the generation of L4 products. For the L4 polar products, after correcting for seasonal bias at Level 2, an OI identical to that of Phase 1 will be conducted. Several strategies will be tested including: different seasonal corrections, use of the estimated SSS i) with or without wind speed retrieval, ii) with or without seasonal correction and iii) with or without absolute bias correction. In the first CRDP, the global product will cover the period 01/2010-10/2022. The research polar product will either cover the period 01/2010-11/2020 if based on the SMOS v671 L2 product or the same period as the global product if the latter is of at least as good quality as v671 derived polar product.

For the CRDP 2, we plan to adjust some components of the radiative transfer model used in the SMOS SSS retrieval and to rerun the L2OS processor using SMOS L1 v7, ERA5 auxiliary parameters and ISAS to derive SMOS OTT, in order to get a more stable SMOS SSS time series.

4.2 CCI C/X-band river plume phase 2 SSS plan

The plan for the algorithm development of the first CDRP of phase-2 includes the following major steps:

Step 1) filtering out/masking the input ΔTb where the Median Absolute Deviation strongly differ between ascending and descending passes before training the NN.

Step 2) use AMSR-E SST as input to the NN SSS inversion algorithms, instead of CCI SST and assess the impact on retrieved SSS quality.

Step 3) NN Retrieval tests will be conducted for ascending and descending passes separately or by merging both passes to determine in which conditions do the NN inversion performs better.

Step 4) Retrieval tests will be conducted with, and, without, these extra polynomial empirical adjustments to determine in which conditions do the NN inversion performs better than our empirical fitting functions based on residual data analyses.

Step 5) we will use the EN4 validated data to best estimate the NN L3 SSS errors and to define quality levels (e.g. as a function of distance to coast, wind regimes, etc ...)

Step 6) Analyses of the representativity error will be conducted for the specific spatial (~60 km) and temporal resolution (monthly) of AMSR-E SSS using high resolution (1/36°) model outputs in the four regions.

For the 2nd CRDP of phase-2, we plan three major steps:

Step 1: Refine algorithms (NN) developed for the four above regions if/when needed (e.g., fresh SSS bias)

Step 2: extension to other potential regional River plume regions including Yangtze and Mekong river plumes.

Step 3: consolidate the regional AMSR-E products by adding WindSat based retrievals if the Windsat Tb can be made available through ESA.

End of document